Demonstration of dispersion gas barometry

Yuanchao Yang,[1,2] Jack A. Stone,[1,*] and Patrick F. Egan[1,†]

[1] *National Institute of Standards and Technology, Gaithersburg, Maryland 20899, USA*
[2] *National Institute of Metrology, Beijing 100029, China*

Realization of the optical pascal has been limited by systematic errors caused by distortion of the optic. In this work, distortion error is circumvented via synchronous measurement of helium refractivity at two optical frequencies. The resultant pressure realization achieves combined standard uncertainty of $5.7 \times 10^{-6} p$, chiefly limited by *ab initio* knowledge of helium dispersion. Two-color measurements are also presented for neon, argon, and nitrogen, which enable semiprimary realization of the pascal in a more practical embodiment. For argon dispersion, measurement and *ab initio* calculation barely agree within mutual expanded uncertainty; experiment is about 16 times more accurate than theory.

I. INTRODUCTION

Mercury manometers and piston gages are the workhorse standards for pressure metrology [1]. In international comparisons, they have demonstrated consistency at the level of $5 \times 10^{-6} p$ [2,3]. But having been perfected over the past 400 and 150 years, respectively, further effort tackling their limitations will yield minimal gains. Already for the piston gage, the past generation of effort in dimensional metrology and flow modeling has not significantly improved the realization [2,4,5].

An alternative route [6] to the pascal is the virial equation of state

$$p = \rho RT(1 + B_\rho \rho + C_\rho \rho^2 + \cdots), \qquad (1)$$

which defines pressure as density ρ at a known temperature T, with deviations from ideal gas behavior described by density virial coefficients B_ρ and C_ρ. The international system of units defines the molar gas constant R as a fixed value without uncertainty. Modern thermometry [7] places the limit of Eq. (1) at $5 \times 10^{-7} T$—an order of magnitude more accurate than the mechanical limits of a piston gage.

For the density in Eq. (1), a precision measurement may be accessed via the extended Lorentz-Lorenz equation,

$$\frac{n^2 - 1}{n^2 + 2} = A_R \rho + B_R \rho^2 + C_R \rho^3 + \cdots \qquad (2)$$

At first order, $\rho \approx (2/3 A_R)(n - 1)$ and the density limit on Eq. (1) is either the measured refractivity $n - 1$ or knowledge of the molar refractivity A_R. (The B_R and C_R are refractivity virial coefficients.) Helium is the gold-standard thermometric gas, because theory claims [8] uncertainty below $10^{-7} A_R$. Consequently, the limit realizing Eq. (1) is measurement of $n - 1$, which has large uncertainty caused by distortion of the optical device when filled with gas.

This work introduces dispersion gas barometry, which realizes the pascal via Eqs. (1) and (2) with uncertainty approaching that of mechanical standards. The method interrogates a Fabry-Perot (FP) cavity at two widely separated laser frequencies and uses the *ab initio* calculation of helium dispersion to simultaneously extract both the gas pressure and distortion coefficient of the cavity. The method is validated by comparing the optical pressure to a mechanically generated pressure at the highest level of accuracy. Finally, the approach is extended to other gases relevant to thermodynamic metrology and the first-order dispersion coefficients of neon, argon, and nitrogen are derived with accuracies exceeding recent *ab initio* calculation by more than an order of magnitude. These coefficients may serve as reference data to establish semiprimary realization of the pascal with gases more practical for metrology.

II. METHOD AND IMPLEMENTATION

This section begins with simplified concepts of how optical pressure may be derived from measurement of refractivity at two separate frequencies. Details behind the experimental implementation are then described. Finally, full equations underlying the analysis are given, which formalize the initial simplified concept.

---

*Retired.
†Contact author: egan@nist.gov

A. Simplified principle

An FP cavity refractometer measures $n - 1 \approx -\Delta f/\nu + \kappa p$, where $\Delta f/\nu$ is the fractional change in the cavity resonance frequency as gas is added and κ is the distortion coefficient. From Eqs. (1) and (2), $n - 1 \approx 3A_R p/(2RT)$, so

$$p\frac{3A_R}{2RT} = -\frac{\Delta f}{\nu} + \kappa p, \qquad (3)$$

with the molar refractivity,

$$A_R(\nu) = A_\epsilon + A_2\bar{\nu}^2 + A_4\bar{\nu}^4 + A_6\bar{\nu}^6 + A_\mu, \qquad (4)$$

having $A_\epsilon \equiv (4\pi/3)N_A\alpha$ from static polarizability α and $A_\mu \equiv (4\pi/3)N_A\chi$ from magnetic susceptibility χ, with the Avogadro constant N_A. The Cauchy coefficients $A_{2,4,6}$ describe polarizability dispersion as a function of reduced frequency $\bar{\nu} \equiv \nu/(10^{14} \text{ Hz})$, with $\nu = c/\lambda$ given by the speed of light in vacuum divided by the wavelength. If refractivity is simultaneously measured at disparate frequencies—say, blue and red—κp mostly cancels from the difference between two Eq. (3) and the optical pressure is (at first order)

$$p_{\text{ops}} = \frac{2RT}{3A_2(\bar{\nu}_{\text{blue}}^2 - \bar{\nu}_{\text{red}}^2)}\left[\left(\frac{\Delta f}{\nu}\right)_{\text{red}} - \left(\frac{\Delta f}{\nu}\right)_{\text{blue}}\right]. \quad (5)$$

A key attribute of Eq. (5) is that measuring the two frequencies in the quotient $\Delta f/\nu$ is independent of a pressure standard. Likewise, for helium, the dispersion polarizability A_2 is known from *ab initio* calculation, which is also independent of pressure. Consequently, Eq. (5) realizes p_{ops} with only a weak dependence on knowledge of pressure.

B. Apparatus and procedure

The present apparatus is the same as for Ref. [9], in which a 15-cm FP cavity made of titania-silicate glass was suspended by wires and temperature stabilized near 303 K. The FP cavity has mirrors that are dual coated for 99.8% reflectivity at 633 nm and 1542 nm. In this work, lasers at the two frequencies have simultaneously interrogated the cavity resonances and change in the respective resonance frequencies (caused by change in gas pressure) has been synchronously measured by two frequency counters. A schematic of the general layout is shown in Fig. 1. The interrogating lasers were an He-Ne laser at 473.61187 THz and an external-cavity diode laser (ECDL) at 194.36862 THz. The reference frequencies against which the change in cavity resonances were compared were two lasers phase locked to a frequency comb. The lasers referenced to the comb were again an He-Ne laser and an ECDL. The frequency comb was stabilized to a global positioning system-disciplined oscillator
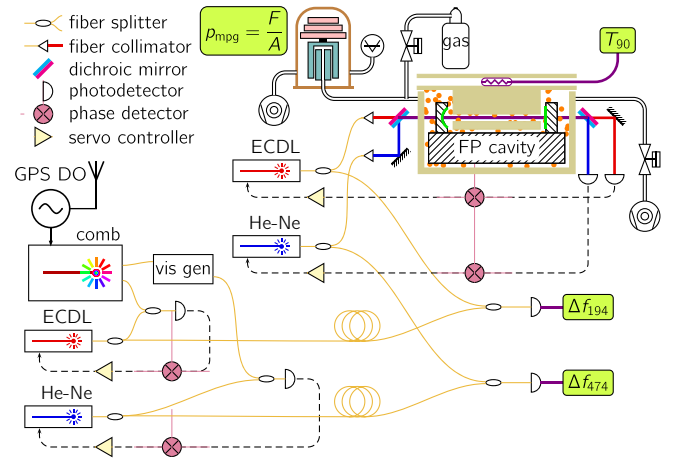

FIG. 1. The general system schematic. Finer details on the optics, the electronics, and the cavity coupling have been omitted.

(GPS DO). Two points are emphasized: (1) the widely separated reference frequencies are phase locked to the same time base, and (2) there is synchronous counting. In this modality, the measurement precision on the difference in resonance frequencies was better than 200 Hz, as limited by fluctuations in the cavity lock points, a consequence of low finesse.

A minor difference over Ref. [9] is that the gas chamber has been redesigned. Differentially pumped o-rings have reduced outgassing to levels of negligible influence. The gas volume surrounding the FP cavity has been reduced by a factor of 8 to mitigate disturbances related to ΔpV heating. This optimization halves the settling-time: 650 s to reach 0.1-mK gradients for $\Delta p = 0.1$ MPa. Moreover, the total thermal disturbance is reduced by a factor of 6: the average cavity temperature changes by less than 5 mK for $\Delta p = 0.1$ MPa. In this new design, the chamber lid protrudes into the open cavity volume, so that the cavity mode and the thermometer are both encapsulated in a block of aluminum, but the thermometer remains in air, outside the pure gas volume. (The Supplemental Material [10] has a three-dimensional drawing that better illustrates this important thermal feature.)

The results presented below will discuss isotherms. An isotherm is a measurement series of quadruplets. A quadruplet means two refractivities, a pressure, and a temperature. The refractivities at the two frequencies have been measured as a function of pressure, at nominally constant temperature. Each gas studied has 100 quadruplets spanning $(0.05 < p < 0.5)$ MPa. The gas temperature was measured by a capsule-type standard platinum resistance thermometer. The gas pressure was generated by a piston gage. The two refractivities were deduced by the change in cavity resonance frequency (details behind the conversion follow next). The measured data and analysis scripts are available from a data repository [11].

C. Detailed analysis

The basic concept of the technique is embodied in the approximate result of Eq. (5). A more exact treatment begins with a refined working equation to determine the refractivity from measurements of the cavity resonant frequencies at vacuum and filled with gas:

$$n - 1 = \frac{\Delta m - \dfrac{\Delta f}{\Delta \nu_{\text{fsr}}} - \dfrac{2(\nu + \Delta f)}{c}\Delta L}{m - 1 + \dfrac{\Delta f}{\Delta \nu_{\text{fsr}}} + \dfrac{\Phi}{\pi} + \dfrac{2(\nu + \Delta f)}{c}\Delta L}, \quad (6)$$

which avails of insights from Ref. [12]. Δm is the change in the mode number caused by the change in the refractive index relative to vacuum and m is the mode number of the cavity resonance frequency ν in vacuum. $\Delta f / \Delta \nu_{\text{fsr}}$ is a quotient of two measured quantities: the change in resonance frequency as gas is added, divided by the cavity-free spectral range. Φ is the Gouy phase. An important feature of Eq. (6) is that a subset of pressures (refractivities) achieve $|\Delta f / \Delta \nu_{\text{fsr}}| < 0.05$ for *both* resonant frequencies. Consequently, the error contribution to $n - 1$ from uncertainty in the measured frequency quotient becomes small; a ratio of integers $\Delta m / (m - 1)$ has no uncertainty.

As the refractometer is filled with gas, the critical variable in Eq. (6) is the change in the cavity length,

$$\Delta L = \Delta L_\kappa + \Delta L_\beta, \quad (7)$$

which is primarily caused by pressure-induced distortion $\Delta L_\kappa = -\kappa p L$, with $\kappa \approx 10^{-11}$ Pa^{-1} a close approximation to the one-dimensional compressibility of titania-silicate glass. For an amorphous solid, κ is relatively large and unpredictable. Consequently, imperfect knowledge of κ has been the hamartia when optical methods have attempted to realize Eq. (1). A secondary complication is $\Delta L_\beta = \beta p \sqrt{t} L$, which accounts for diffusion over time t via the fit parameter $\beta \approx 3 \times 10^{-14}$ Pa^{-1} h$^{-1/2}$. Diffusion in titania-silicate glass is a problem specific to the measurement of helium and $-\Delta L_\kappa \gtrsim 10^2 \Delta L_\beta$. (The Supplemental Material contains more detail about β and helium diffusion [10].)

Dispersion gas barometry circumvents ΔL by first assuming that cavity distortion (and diffusion) is the same at both resonant frequencies. The next assumption is that measured refractivities from Eq. (6) for two frequencies should be equivalent to calculated refractivities

$$n - 1 = \mathcal{A}p + \mathcal{B}p^2 + \mathcal{C}p^3 \quad (8)$$

at the same two frequencies. The proportionality coefficients are

$$\mathcal{A} = \frac{3}{2(RT)} A_{\text{R}},$$

$$\mathcal{B} = \frac{3}{8(RT)^2}\left(A_{\text{R}}^2 - 4A_{\text{R}}B_\rho + 4B_{\text{R}}\right),$$

$$\mathcal{C} = \frac{3}{16(RT)^3}\left[5A_{\text{R}}^3 - 4A_{\text{R}}^2 B_\rho \right.$$
$$\left. + 4A_{\text{R}}(4B_\rho^2 + B_{\text{R}} - 2C_\rho) + 8(-2B_{\text{R}}B_\rho + C_{\text{R}})\right], \quad (9)$$

in which the frequency dependencies of $A_{\text{R}}(\nu)$ and $B_{\text{R}}(\nu)$ are implicit. Equation (8) and its proportionality coefficients result from expressing density as a series function of $p/(RT)$ via Eq. (1) and then using that expression to eliminate density from Eq. (2). The derivation also approximates the Lorentz-Lorenz quotient as a third-order series in $n - 1$.

The final analysis equates the right-hand sides of Eqs. (6) and (8) to one another at both frequencies. Thereby, a pair of simultaneous equations are configured, which may be solved for two unknowns at every quadruplet. The choice of what is unknown in Eq. (6) or Eq. (8) depends on the gas being studied, as explained next.

III. RESULTS

The results of this work are twofold and concern helium first, followed by three other gases—neon, argon, and nitrogen. All analyses rest on Eqs. (6) and (8). The difference between the analyses is what is treated as unknown in the pair of simultaneous equations. First, the helium measurements are presented as a solution for ϵ_p and ΔL. The main result is ϵ_p, which may either be interpreted as a primary realization of the optical pascal or as a stringent validation of helium dispersion theory. Second, the other gas measurements are presented as a solution for A_ϵ and A_2, the leading terms in Eq. (4). These results may either be interpreted as reference data allowing semiprimary realization of the optical pascal or as benchmark values to assist new developments in *ab initio* calculation.

A. Helium: Realization of the optical-pressure scale

The helium analysis sets ΔL in Eq. (6) as one unknown and treats p in Eq. (8) as the second unknown. Numerically, the approach is implemented by adding a pressure-calibration parameter ϵ_p to the series variable of Eq. (8); i.e., $(1 + \epsilon_p)p$. The roots of the simultaneous equations produce ΔL and ϵ_p, and the product $(1 + \epsilon_p)p \equiv p_{\text{ops}}$ is the optical pressure conceptualized in Eq. (5). In this work, the preestimated p is provided at the highest level of accuracy, as force over area in a mechanical pressure generator [5]. Consequently, the pressure-calibration parameter ϵ_p may be understood as equivalence (or deviation) between the independent optical and mechanical pressure scales. (If dispersion gas barometry were executed with an inaccurate pressure transducer, the value taken by ϵ_p would calibrate the transducer to the optical-pressure scale.) One major
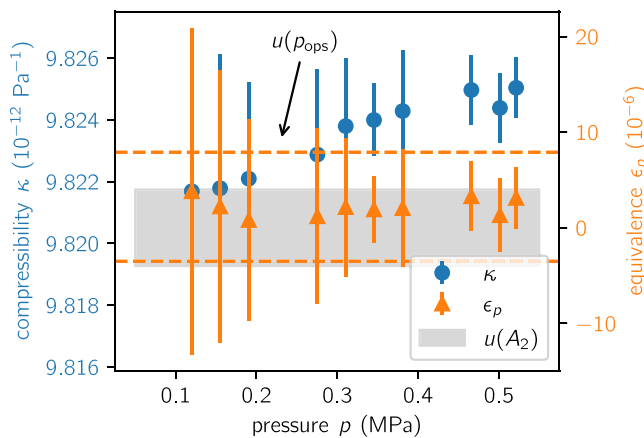
FIG. 2. Parameters κ and ϵ_p deduced by measurement of helium dispersion. The error bars span standard deviations on ten repeats at each set pressure. The dashed lines show combined uncertainty in the experimentally realized optical-pressure scale; the shaded area denotes the contributed uncertainty of dispersion theory.

attraction of dispersion gas barometry is the fact that the ϵ_p needed to calibrate the pressure input to Eq. (8) is identified independent of compressibility, diffusion, and expansivity. Furthermore, the ΔL model of Eq. (6) could be any complex length change, so long as it equally affects the cavity length at both resonant frequencies. It is emphasized that solving for $(1 + \epsilon_p)p$ only needs the preestimated p to be accurate enough to identify Δm in (6), which corresponds to a trivial ± 3.2 kPa.

Results of the implementation described above are shown in Fig. 2 for a helium isotherm measured near 303 K. The result for one unknown is presented as determination of an effective compressibility $\kappa = (-\Delta L + \Delta L_\beta)/(p_{\text{ops}}L)$ but the actual value deduced is ΔL. From Eq. (7), deriving κ requires correction for diffusion of helium [10] and an estimate of the geometric cavity length. The derived κ data suggest a fractional increase in compressibility as a function of pressure approximately 4×10^{-4} MPa^{-1}. Such a trend is within the precision of the present demonstration, but it is notable that fused silica glass is expected [13] to exhibit 1.6×10^{-4} MPa^{-1}. (Titania-silicate glass is a binary composition, nominally 92% silica and 8% titania.)

Some comments about the result of Fig. 2 highlight the remarkable precision. First, $3A_2(4.74^2 - 1.94^2)/(2RT) \approx 1.5 \times 10^{-12}$ /Pa, so the effect of dispersion on the resonance frequencies is almost an order of magnitude smaller than the effect of compressibility! The result of Fig. 2 means that fractional changes in the resonance frequency of an FP cavity have been accounted for within 10^{-12}. This precision is not too challenging for an isolated and permanently evacuated cavity. By contrast, the present work represents a quasidynamic measurement over analysis intervals of 1 h, with disturbances from pV work,

compressibility and expansivity, and diffusion. In terms of ΔL in Eq. (6), for all 100 quadruplets solved, the standard deviation on residuals from a linear fit in pressure is 18 pm. It is worth translating two-color performance into conventional single-wavelength refractometry: in helium, $dn/dp \approx 3.2 \times 10^{-10}$ Pa^{-1}, so $\Delta nL \approx 12$ μm at $p = 0.25$ MPa and $L = 0.15$ m. The 18-pm precision on ΔL means that the two-color method delivers distortion-corrected accuracy in helium at the level of $1.5 \times 10^{-6}(n - 1)$. This performance has been achieved despite the fact that the geometric length of the cavity distorts by 370 nm and experiences a 0.75-nm/$\sqrt{\text{h}}$ diffusion transient. The accuracy would increase as pressure increases but an account for nonlinearity [13] in $\Delta L(p)$ would also be needed.

The equivalence parameter in Fig. 2 is $\epsilon_p = (2.2 \pm 5.7) \times 10^{-6}$, with the first number denoting the weighted average of the data and the second number the estimated standard uncertainty. The ϵ_p result has two interpretations. The first interpretation is that the newly realized optical-pressure scale agrees with the mechanical realization $p = F/A$ within mutual uncertainty. The result is noteworthy for international pressure metrology: arguably, the optical-pressure scale now exceeds what is realistic by mechanical means across 6 orders of magnitude ($10^{-6} < p < 1$) MPa. The second interpretation of the ϵ_p result is that experiment has validated helium dispersion within the uncertainty of *ab initio* theory. The result is significant regarding the postulated retardation correction [14] to A_2 over what was originally estimated [8]. The retardation correction is $-2.4 \times 10^{-5}A_2$, which is a $4 \times 10^{-5}p$ influence on the ϵ_p result for the frequencies of the present work. In the context of metrological stress tests [15], helium theory passes once again but it is the limit on a dispersive realization of the pascal.

The combined standard uncertainty on this realization of the optical pascal is $5.7 \times 10^{-6}p$ and a detailed discussion is given in the Supplemental Material [10]. Here is a synopsis. The main contributor to uncertainty is theoretical knowledge of helium dispersion at $4.0 \times 10^{-6}p$. Two smaller contributors are statistical uncertainty in the apparatus ($3.0 \times 10^{-6}p$) and uncertainty in the measurement of gas temperature ($2.5 \times 10^{-6}p$), which employs the correction to thermodynamic temperature [16] near 303 K. The two smaller contributors seem straightforward to reduce. Uncertainty in the measured gas temperature would be halved by operating near 273 K. For statistical uncertainty, the error bars in Fig. 2 show increased deviation at low pressure. The origin is frequency error, caused by irreproducibility of the cavity lock point. A higher-finesse cavity is likely to reduce statistical uncertainty at lower pressure. Further improvement might come via Eq. (5), which suggests that a factor-of-3 increase in the pressure signal would be obtained if the "blue" laser were closer to 750 THz.

B. Optical properties of practical metrology gases

The gases neon, argon, and nitrogen are more practical for metrology—their higher polarizability improves performance at low pressures, they are less affected by contaminants, and they do not permeate silicate glasses. Ideally, the parameters of Eq. (4) for the practical metrology gases would be established by consensus measurements. The following results contribute toward that long-standing [6,17] goal.

Like helium, analysis of the other gases also configures the right-hand sides of Eqs. (6) and (8) as a pair of simultaneous equations. However, for the other gases, the ΔL in Eq. (6) and ϵ_p in (8) are treated as known parameters from the helium measurement above. Strictly, $\Delta L \rightarrow \Delta L_\kappa$ because $\beta = 0$ for other gases. The ΔL_κ is derived from the helium measurement via Eq. (7), with ΔL_β identified by regression of transient data to a diffusion model [10]. The ΔL_κ is assumed to be species independent. Since ΔL and ϵ_p are known parameters, the simultaneous equations are set up with Eq. (8) being a variable function of Eq. (4), in which A_ϵ and A_2 are the two unknowns found by root solving.

The results of the isotherms near 303 K are shown in Fig. 3, which showcases the exquisite precision of the method—better than 10^{-6} on A_ϵ and 10^{-5} on A_2. Trends as a function of pressure in Fig. 3 are caused by residual error in the second-order term of Eq. (8). An $A_\epsilon(p)$ trend would be chiefly influenced by error in the second density virial coefficient B_ρ. The analysis has used Ref. [18] for neon and Ref. [9] for argon and nitrogen. The weak trends on $A_\epsilon(p)$ for all three gases give confidence that B_ρ are accurate. The deduced $A_2(p)$ is influenced by error in the frequency dependence of the second refractivity virial coefficient $B_R(\nu) = B_\epsilon + B_R^{(2)}\bar{\nu}^2$. The trend in the $A_2(p)$ value for nitrogen reflects a complete lack of knowledge on $B_R^{(2)}$, which has been set to zero. For neon and argon, there is good theoretical knowledge [19] of $B_R(\nu)$. However, correlation between B_ρ and B_R preclude the practicality of deriving $B_R^{(2)}$ from the observed trends in $A_2(p)$. (Solving two simultaneous equations at two frequencies allows two unknowns to be uniquely identified. A determination of $B_R^{(2)}$ might be possible with a third frequency.)

C. Summary of results

The A_ϵ and A_2 deduced from the present work are compared with the literature in Table I. From the previous subsection, the results for neon, argon, and nitrogen have employed $\epsilon_p = 2.2 \times 10^{-6}$ and the measurements are traceable to p_{ops}. The metrological nuance is emphasized: the results for neon, argon, and nitrogen in Table I are reported on the optical-pressure scale (i.e., relative to the *ab initio* calculation of helium dispersion) and are independent of the piston gage. For neon and argon, Table I shows
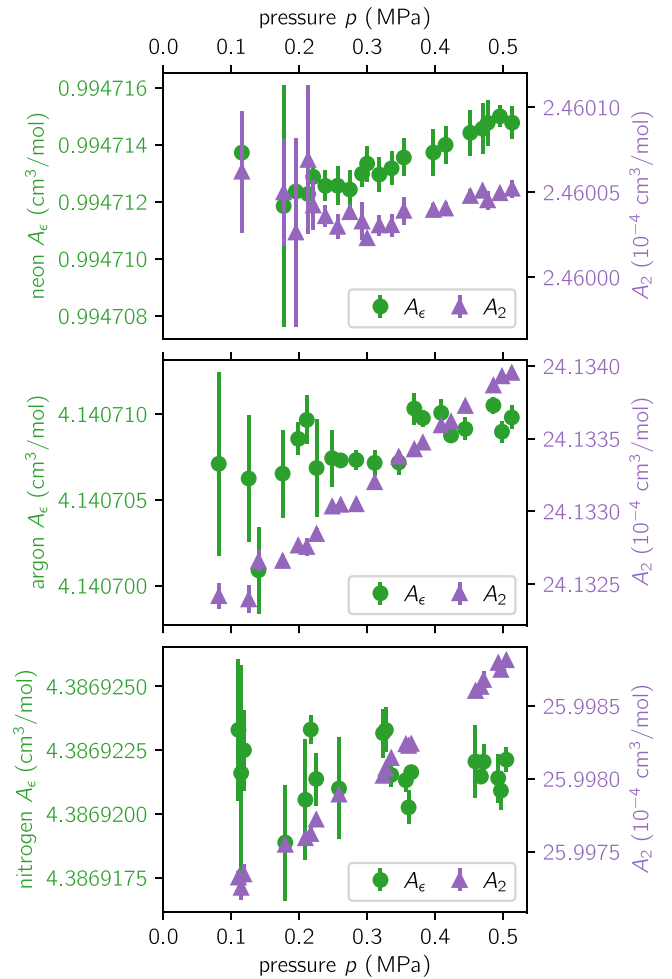

FIG. 3.   The dispersion polarizability for the practical metrology gases. The error bars span standard deviations on five repeats at each set pressure.

that the present work agrees well with the latest *ab initio* theory [8,14,20,21,24] and the highly accurate capacitance measurement of Gaiser and Fellmuth [17]. Nitrogen lacks an *ab initio* cross-check but the present result agrees with a refractivity measurement at 1550 nm [25] relative to argon [17].

The measurement uncertainty on A_ϵ and A_2 is described in the Supplemental Material [10]. Here is a synopsis. Uncertainty on A_ϵ is chiefly dominated by the measured (optical) pressure, which at $5.7 \times 10^{-6}A_\epsilon$, is limited by the *ab initio* knowledge of helium dispersion. Uncertainty in the measured temperature is also significant at $2.5 \times 10^{-6}A_\epsilon$. For the case of neon, uncertainties arising from impurity ($4.0 \times 10^{-6}A_\epsilon$) and the κ deduced from helium measurement ($3.3 \times 10^{-6}A_\epsilon$) are both larger than uncertainty in the measured temperature. Furthermore, for all three gases, this work must assume something for A_μ in Eq. (4). The noble gases have A_μ calculated by *ab initio* methods [26,27] and calculated results for nitrogen are being

TABLE I. A comparison of the literature with the present work for the coefficients describing dispersion polarizability in Eq. (4). The numbers in parentheses denote standard uncertainty, where available.

Gas	$A_\epsilon/(cm^3/mol)$	$A_2/(10^{-4} cm^3/mol)$	Ref.
Ne	0.9946(1)	2.461(5)	Theoretical [20]
	0.994711(2)	. . .	Experimental [17]
	0.994709(8)	2.46000(8)	This work
Ar	4.1408(7)	24.16(1)	Theoretical [21]
	4.14069(1)	. . .	Experimental [17]
	4.14070(3)	24.1320(8)	This work
N_2	4.388	25.70	Experimental [22]
	4.3877(2)	. . .	Experimental [23]
	4.38692(3)	25.997(5)	This work
He	0.51725408(5)	1.332465(5)	Theoretical [8,14,24]
	0.517254(1)	. . .	Experimental [17]
	. . .	1.332468(6)	This work

finalized [28]. Nevertheless, there is an unresolved discrepancy between old experiment and recent theory [27], corresponding to about $2 \times 10^{-6} A_\epsilon$. (The experimental situation for A_μ is not healthy—the most recent, and possibly discrepant, measurement dates from 60 years ago.) Consequently, capacitance measurements that directly access A_ϵ will be more reliable than the derived values of this work.

By contrast, uncertainty on A_2 is dominated by measurement statistics plus systematic error in A_4 and A_6. For neon and argon, combined uncertainty is about $3.5 \times 10^{-5} A_2$, with nominally equivalent contributions from statistic and systematic errors. Statistics might be improved with a high-finesse cavity but improvements in A_4 and A_6 seem unlikely, since knowledge is already at the limit of modern theory [20,21]. Nevertheless, the A_2 values deduced from this work are 66 and 16 times more accurate than *ab initio* theory of neon and argon, respectively. For nitrogen, the combined uncertainty is $20.0 \times 10^{-5} A_2$ and is completely dominated by systematic error in the A_4 and A_6 values derived from the dipole oscillator strength sums [22]. Fortunately, *ab initio* developments under way [28] are likely to provide more accurate A_4 and A_6 values and reduce the uncertainty of A_2 derived from this work by a factor of 2 or more.

Finally, for completion, Table I also lists the A_2 result for helium. Effectively, this is a third approach to the simultaneous equations of Eqs. (6) and (8). Removing circularity between variables prescribes $\epsilon_p = 0$, so ΔL from Eq. (6) and A_2 from Eq. (8) may be solved. The A_ϵ must be set to the *ab initio* value, which explains the blank entry in Table I.

IV. CONCLUSIONS

This work has presented the first demonstration of dispersion gas barometry—an optical realization of the pascal based on helium refractivity at known temperature, simultaneously measured at two widely separated frequencies. A crucial attribute of the method is that the realization has no significant dependence on the quantity of like kind (i.e., pressure). More fundamentally, the work has advanced knowledge of gas dispersion. For helium, the work has validated the *ab initio* calculation of polarizability dispersion and corroborated the need for a retardation correction. Notwithstanding the breakthrough results already attained, gains in performance are foreseen through higher cavity finesse and shorter wavelength.

Results have also been presented for the dispersion of neon, argon, and nitrogen, formulated as Cauchy coefficients A_ϵ and A_2. For the dispersion coefficient A_2, the accuracy of this work exceeds both *ab initio* calculation and prior measurement by more than an order of magnitude. The Cauchy coefficients derived in this work have been established on the optical-pressure scale and are independent of piston gages and mercury manometers. These Cauchy coefficients allow semiprimary realization of the pascal in a more practical embodiment; e.g., via a single-laser refractometer in argon without a frequency comb.

DATA AVAILABILITY

The data that support the findings of this paper are openly available [11].

[1] C. R. Tilford, in *Determination of Thermodynamic Properties*, edited by B. W. Rossiter and R. C. Baetzold, Physical Methods of Chemistry, Vol. 6, 2nd ed. (Wiley, Hoboken, New Jersey, 1992), chapter 2, p. 101.

[2] G. F. Molinar, B. Rebaglia, A. Sacconi, J. C. Legras, G. P. Vailleau, J. W. Schmidt, J. R. Stoup, D. R. Flack, W. Sabuga, and O. Jusko, CCM key comparison in the pressure range 0.05 MPa to 1 MPa (gas medium, gauge mode). Phase A1: Dimensional measurements and calculation of effective area, Metrologia **36**, 657 (1999).

[3] M. Perkin, A. Picard, M. Lecollinet, K. Fen, M. Sardi, A. Miiller, A. Agarwal, M. Jescheck, and C. Wüthrich, Final report on CCM key comparison CCM.P-K2: Pressure

(10 kPa to 120 kPa) absolute mode, Metrologia **45,** 07002 (2008).

[4] T. Zandt, W. Sabuga, C. Gaiser, and B. Fellmuth, Measurement of pressures up to 7 MPa applying pressure balances for dielectric-constant gas thermometry, Metrologia **52,** S305 (2015).

[5] P. F. Egan, E. S. Stanfield, J. R. Stoup, and C. W. Meyer, Conversion of a piston-cylinder dimensional dataset to the effective area of a mechanical pressure generator, Metrologia **61,** 065004 (2024).

[6] J. W. Schmidt, R. M. Gavioso, E. F. May, and M. R. Moldover, Polarizability of helium and gas metrology, Phys. Rev. Lett. **98,** 254504 (2007).

[7] M. R. Moldover, W. L. Tew, and H. W. Yoon, Advances in thermometry, Nat. Phys. **12,** 7 (2016).

[8] M. Puchalski, K. Piszczatowski, J. Komasa, B. Jeziorski, and K. Szalewicz, Theoretical determination of the polarizability dispersion and the refractive index of helium, Phys. Rev. A **93,** 032515 (2016).

[9] P. F. Egan and Y. Yang, Optical $n(p, T_{90})$ measurement suite 1: He, Ar, and N_2, Int. J. Thermophys. **44,** 181 (2023).

[10] See the Supplemental Material at http://link.aps.org/supplemental/10.1103/z9zz-lqzh for a derivation of the refractometer working equation, plumbing details, lessons learned from an unstable cavity, the helium diffusion model, efforts made to ensure helium purity, and the uncertainty analysis. The Supplemental Material cites Refs. [29–38].

[11] The measured data and analysis scripts are available from the NIST data repository (2025), https://doi.org/10.18434/mds2-3695.

[12] I. Silander, J. Zakrisson, V. S. de Oliveira, C. Forssén, A. Foltynowicz, T. Rubin, M. Zelan, and O. Axner, *In situ* determination of the penetration depth of mirrors in Fabry-Perot refractometers and its influence on assessment of refractivity and pressure, Opt. Express **30,** 25891 (2022).

[13] M. Vukcevich, A new interpretation of the anomalous properties of vitreous silica, J. Non-Cryst. Solids **11,** 25 (1972).

[14] K. Pachucki and M. Puchalski, Refractive index and generalized polarizability, Phys. Rev. A **99,** 041803 (2019).

[15] C. Gaiser, B. Fellmuth, and W. Sabuga, Primary gas pressure standard passes next stress test, Ann. Phys. **534,** 2200336 (2022).

[16] C. Gaiser, B. Fellmuth, R. M. Gavioso, M. Kalemci, V. Kytin, T. Nakano, A. Pokhodun, P. M. C. Rourke, R. Rusby, F. Sparasci, P. P. M. Steur, W. L. Tew, R. Underwood, R. White, I. Yang, and J. Zhang, 2022 update for the differences between thermodynamic temperature and ITS-90 below 335 K, J. Phys. Chem. Ref. Data **51,** 043105 (2022).

[17] C. Gaiser and B. Fellmuth, Polarizability of helium, neon, and argon: New perspectives for gas metrology, Phys. Rev. Lett. **120,** 123203 (2018).

[18] R. Hellmann, C. Gaiser, B. Fellmuth, T. Vasyltsova, and E. Bich, Thermophysical properties of low-density neon gas from highly accurate first-principles calculations and dielectric-constant gas thermometry measurements, J. Chem. Phys. **154,** 164304 (2021).

[19] G. Garberoglio and A. H. Harvey, Path-integral calculation of the second dielectric and refractivity virial coefficients of helium, neon, and argon, J. Res. Natl. Inst. Stand. Technol. **125,** 125022 (2020).

[20] M. Lesiuk, M. Przybytek, and B. Jeziorski, Theoretical determination of polarizability and magnetic susceptibility of neon, Phys. Rev. A **102,** 052816 (2020).

[21] M. Lesiuk and B. Jeziorski, First-principles calculation of the frequency-dependent dipole polarizability of argon, Phys. Rev. A **107,** 042805 (2023).

[22] A. Kumar and W. J. Meath, Constrained anisotropic dipole oscillator strength distribution techniques, and reliable results for anisotropic and isotropic dipole molecular properties, with applications to H_2 and N_2, Theor. Chim. Acta **82,** 131 (1992).

[23] J. W. Schmidt and M. R. Moldover, Dielectric permittivity of eight gases measured with cross capacitors, Int. J. Thermophys. **24,** 375 (2003).

[24] M. Puchalski, K. Szalewicz, M. Lesiuk, and B. Jeziorski, QED calculation of the dipole polarizability of helium atom, Phys. Rev. A **101,** 022505 (2020).

[25] I. Silander, J. Zakrisson, O. Axner, and M. Zelan, Realization of the pascal based on argon using a Fabry-Perot refractometer, Opt. Lett. **49,** 3296 (2024).

[26] M. Puchalski, M. Lesiuk, and B. Jeziorski, Relativistic treatment of the diamagnetic susceptibility of helium, Phys. Rev. A **108,** 042812 (2023).

[27] M. Lesiuk and B. Jeziorski, Diamagnetic susceptibility of neon and argon including leading relativistic effects, Phys. Rev. A **109,** 012820 (2024).

[28] M. Lesiuk and J. Lang, Atomic Bethe logarithm in the mean-field approximation, Phys. Rev. A **108,** 042817 (2023), Calculated A_μ data for nitrogen at: https://doi.org/10.5281/zenodo.10960043.

[29] J. R. Lawall, High resolution determination of radii of curvature using Fabry-Perot interferometry, Meas. Sci. Technol. **20,** 045302 (2009).

[30] J. Crank, *The Mathematics of Diffusion* (Clarendon Press, Oxford, 1975), 2 ed., chapter 5.

[31] S. Avdiaj, Y. Yang, K. Jousten, and T. Rubin, Note: Diffusion constant and solubility of helium in ULE glass at 23 °C, J. Chem. Phys. **148,** 116101 (2018).

[32] P. F. Egan and Y. Yang, Optical $n(p, T_{90})$ measurement suite 2: H_2O and D_2O, Int. J. Thermophys. **45,** 89 (2024).

[33] J. Rychlewski, Frequency dependent polarizabilities for the ground state of H_2, HD, and D_2, J. Chem. Phys. **78,** 7252 (1983).

[34] P. Czachorowski, M. Przybytek, M. Lesiuk, M. Puchalski, and B. Jeziorski, Second virial coefficients for ^{4}He and ^{3}He from an accurate relativistic interaction potential, Phys. Rev. A **102,** 042810 (2020).

[35] D. Binosi, G. Garberoglio, and A. H. Harvey, Third density and acoustic virial coefficients of helium isotopologues from *ab initio* calculations, J. Chem. Phys. **160,** 244305 (2024).

[36] G. Garberoglio, A. H. Harvey, J. Lang, M. Przybytek, M. Lesiuk, and B. Jeziorski, Path-integral calculation of the third dielectric virial coefficient of helium based on *ab initio* three-body polarizability and dipole surfaces, J. Chem. Phys. **161,** 144111 (2024).

[37] C. Barter, R. G. Meisenheimer, and D. P. Stevenson, Diamagnetic susceptibilities of simple hydrocarbons and volatile hydrides, J. Phys. Chem. **64,** 1312 (1960).

[38] G. G. Havens, The magnetic susceptibilities of some common gases, Phys. Rev. **43,** 992 (1933).

Supplement to: Demonstration of dispersion gas barometry

Yuanchao Yang [1,2] Jack A. Stone [1,*], Patrick F. Egan [1,†]

[1] *National Institute of Standards and Technology, Gaithersburg, MD 20899, USA*
[2] *National Institute of Metrology, Beijing, 100029, China*

I.   REFRACTOMETER WORKING EQUATION

The resonance condition of a Fabry–Perot (FP) cavity at vacuum satisfies the roundtrip phase

$$2\pi m = \frac{4\pi L \nu}{c} + 2\phi - 2\Phi, \tag{S1}$$

with m the integer mode number, L the cavity length (geometric separation between the front facets of the mirrors), and $\nu_{\mathrm{vac}} = c/\lambda$ is laser frequency given by speed of light in vacuum c divided by wavelength λ. In gas, ignoring the pressure-induced decrease in cavity length, the phase condition is

$$2\pi(m + \Delta m) = \frac{4\pi n L(\nu + \Delta f)}{c} + 2(\phi + \Delta \phi) - 2\Phi. \tag{S2}$$

Throughout this work, the convention used for all Δ quantities is gas relative to vacuum; i.e., $\Delta m = m_{\mathrm{gas}} - m_{\mathrm{vac}}$, $\Delta f = \nu_{\mathrm{gas}} - \nu_{\mathrm{vac}}$, etc. The mirror phase shift (high index layer facing the incident laser)

$$\phi = \pi + n\alpha(\nu - \nu_c), \tag{S3}$$

has model parameters for dispersion $\alpha = \mathrm{d}\phi/\mathrm{d}\nu$ and center frequency ν_{c}. The (S3) is the phase shift model for one mirror; the factor 2ϕ appears in (S1) because the cavity is formed by two mirrors. For a homogeneous plano-concave cavity assembly with uniform pressure applied to all surfaces, the Gouy phase $\Phi \approx \arcsin(\sqrt{L/r})$ does not change with pressure. (In this work, the Gouy phase $\Phi = \pi\Delta\nu_{00-01}/\Delta\nu_{\mathrm{fsr}}$ is a measured quantity, given by the frequency difference between the TEM_{00} and TEM_{01} modes divided by the free spectral range [S1]. The measured quantity is 9.3 % smaller than what is estimated from the nominal radius of curvature r.) Subtract (S1) from (S2) and solve for refractivity:

$$n - 1 = \frac{c}{\nu + \Delta f}\left(\frac{\Delta m}{2L} - \frac{\Delta \phi}{2\pi L} - \frac{\Delta f}{c}\right). \tag{S4}$$

The (S4) is a conventional expression [S2], noting $\nu + \Delta f \equiv \nu_{\mathrm{gas}}$. For accurate work, the shortcoming of (S4) is the need to know something about $\Delta\phi$, which would be subject to manufacture tolerances. Insights from Silander et al. [S3] go further:

1. The geometric length of the cavity

$$L = \frac{c}{2\Delta\nu_{\mathrm{fsr}}} - \frac{\alpha c}{2\pi}, \tag{S5}$$

   may be inferred from the measured free spectral range $\Delta\nu_{\mathrm{fsr}}$ together with the mirror stack model estimate of α. Substituting (S5) into (S1) identifies the cavity mode number at vacuum

$$m = \left\lfloor \frac{\nu}{\Delta\nu_{\mathrm{fsr}}} + \frac{\pi - \alpha\nu_{\mathrm{c}}}{\pi} - \frac{\Phi}{\pi} \right\rceil \tag{S6}$$

   as the nearest integer. The mirror phase shift may then be expressed

$$\phi = \pi m - \frac{2\pi L \nu}{c} + \Phi. \tag{S7}$$

---

* retired
† egan@nist.gov

2. From (S3), two resonant frequencies, one at gas and one at vacuum, have

$$\Delta\phi = n\alpha\Delta f + (n-1)(\phi - \pi). \tag{S8}$$

3. Plug the expressions for L from (S5) and $\Delta\phi$ from (S8) into the $n-1$ of (S4):

$$n - 1 = \frac{\Delta m - \dfrac{\Delta f}{\Delta\nu_{\text{fsr}}}}{m - 1 + \dfrac{\Delta f}{\Delta\nu_{\text{fsr}}} + \dfrac{\Phi}{\pi}}. \tag{S9}$$

The requirement for preknowledge of α in (S5) and the product $\alpha\nu_{\text{c}}$ in (S6) above means that ϕ identified by (S7) is a composite value, and nothing independent is known about α or ν_{c} for the mirror model of (S3). However, the formulation of (S9) offers a few important features:

- The expression is mostly independent of mirror phase shift. Neither α nor ν_{c} appear in the formula.

- Along an isotherm, certain pressures at roughly regular intervals produce $\Delta f \to 0$, and $n - 1 \approx \Delta m/(m-1)$ becomes a quotient of two integers *which have no uncertainty.* For two-color measurement, pressures generated by a mass set generally will not find $\Delta f \to 0$ at both frequencies. Crucially, however, selecting pressures that minimize Δf at both frequencies reduces the contribution of $u(\Delta\nu_{\text{fsr}})$ to the measurement of refractivity.

- Surprisingly, the (S9) is exactly equivalent to (S4) and Ref. [S2].

$$\frac{\Delta m - \dfrac{\Delta f}{\Delta\nu_{\text{fsr}}}}{m - 1 + \dfrac{\Delta f}{\Delta\nu_{\text{fsr}}} + \dfrac{\Phi}{\pi}} \equiv \frac{\Delta m\Delta\nu_{\text{fsr}} - \Delta f}{(\nu + \Delta f) - \dfrac{\epsilon_\alpha}{1 + \epsilon_\alpha}\nu_{\text{c}}}, \tag{S10}$$

with $\epsilon_\alpha = c\alpha/(2\pi L)$. However, the presence of α and ν_{c} in the denominator of the right-hand side is problematic for two-color measurements because the mirror phase shift is uncertain and different at both resonant frequencies. The analytically equivalent expressions disagree because of imperfect knowledge of the mirror phase shift. Best knowledge of α and ν_{c} comes from the coating manufacturer. For the two-color application, the right-hand side differs from the left by $2.7\times10^{-6}\cdot A_\epsilon$ and $1.0\times10^{-4}\cdot A_2$, solely caused by error in knowledge of α and ν_{c}. Crucially, for the helium analysis, a 10 % error in α would cause the right-hand side to give error $1.7 \times 10^{-4} \cdot p_{\text{ops}}$.

- Finally, the full working equation accounts for the change in cavity length in gas

$$2\pi(m + \Delta m) = \frac{4\pi n(L + \Delta L)(\nu + \Delta f)}{c} + 2(\phi + \Delta\phi) - 2\Phi. \tag{S11}$$

A derivation as outlined above produces the result used in the main text:

$$n - 1 = \frac{\Delta m - \dfrac{\Delta f}{\Delta\nu_{\text{fsr}}} - \dfrac{2(\nu + \Delta f)}{c}\Delta L}{m - 1 + \dfrac{\Delta f}{\Delta\nu_{\text{fsr}}} + \dfrac{\Phi}{\pi} + \dfrac{2(\nu + \Delta f)}{c}\Delta L}. \tag{S12}$$

The change in cavity length $\Delta L = \Delta L_\kappa + \Delta L_\beta$ is general, and not specific to the models used for distortion $\Delta L_\kappa = -\kappa pL$ or diffusion $\Delta L_\beta = \beta p\sqrt{t}L$. The benefit of the implicit solution using a generalized ΔL is that an explicit solution using $\kappa p = -\Delta L_\kappa/L$ requires knowledge of L, which would reintroduce a dependence on the mirror phase shift via (S5). In the main text, the two-color measurement of helium actually deduces ΔL, and is independent of the mirror phase shift.

II. PLUMBING AND THERMALS

An exploded view of the main plumbing parts of the apparatus is shown in Fig. S1. The fittings to the chamber include two windows, a gas and a vacuum flange, and the chamber lid. All five connections are differential pumped o-rings, with the pumped volume contiguous between all fittings and plumbed with a single run of 3 mm diameter plastic tubing.

The cavity was suspended by wires inside an aluminum chamber. The key feature is the chamber lid protrudes into the chamber, so that the cavity mode (the laser beam resonating between the mirrors) was enclosed inside a bore. The chamber lid also has a bore on the ambient side for the capsule standard platinum resistance thermometer (cSPRT). Therefore, both the cavity mode (optical thermometer) and the cSPRT (resistance thermometer) were enclosed in the same high thermal conductivity block.

The relevant finite-element results of this arrangement are also shown Fig. S1, for an argon charge to 0.1 MPa. The quarter-section gas volume shown on top left is 25 mL. The contour plot shows a fairly isothermal argon volume after only 360 s of settling. The image is also annotated with the location of three critical areas of the model: "cavity mode" is the average temperature along a line through the gas volume, "cSPRT" is a stainless steel sheath embedded in the aluminum chamber lid (in ambient), and the "glass cavity" is the average temperature of a glass solid suspended in the argon volume.

The plot at top right of Fig. S1 shows temperature gradients after the gas fill as a function of time. The two critical gradients are those that exist between (i) the cavity mode and cSPRT, and (ii) the glass cavity and the cSPRT. The former gradient would be a first-order error, representing a systematic error between the sensed temperature and the (optical) gas temperature. The gradient between the glass cavity and the cSPRT is a second-order error only relevant as $p < 0.05$ MPa, and relates to compensating the length of the cavity for thermal expansion. The finite-element result on the top right Fig. S1 shows time-constants of 230 s for the cavity mode gradient, and 1000 s for the glass gradient. For a 0.1 MPa argon fill, the time
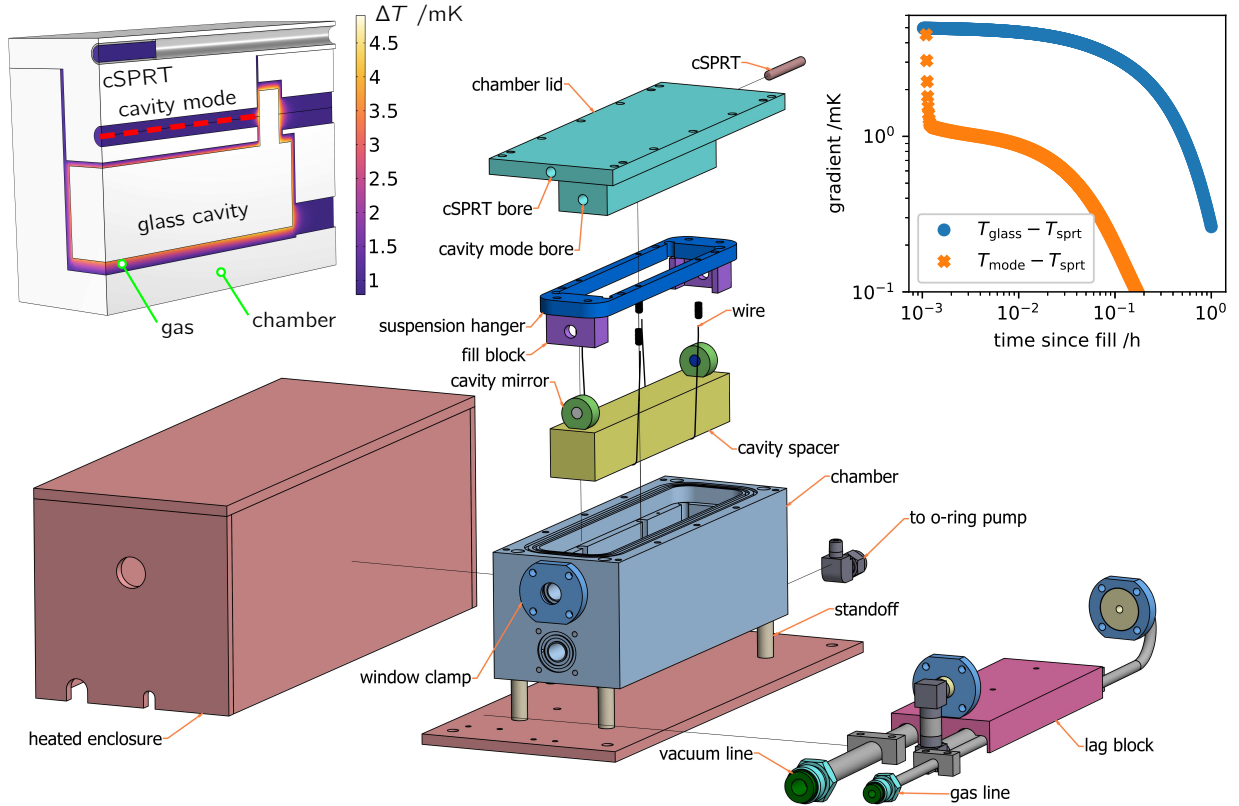

FIG. S1. Detailed view of the apparatus components. Top left is a contour plot of thermal gradients in the argon volume, 360 s after a 0.1 MPa fill. Top right is gradients over time between the cavity mode T_{mode} or glass cavity T_{glass}, relative to the thermometer T_{sprt}.

required to reach 0.1 mK gradients between the cavity mode and cSPRT is 650 s. Simulations for helium are not shown in Fig. S1, but a 0.1 MPa helium fill takes 430 s to equilibrate within 0.1 mK. The settling time is dominated by heat transfer between the two critical areas within the aluminum chamber lid, rather than the thermal conductivity of the test gas.

III.   LESSONS FROM AN UNSTABLE CAVITY

Initial investigations employed a separate FP cavity which was 122 mm long. This FP$_{122}$ cavity is similar to the FP$_{150}$ cavity used in the main text: both cavities were built in 2016 using spacers from the same material batch with mirrors from the same coating run, and both cavities are of the "fully open" geometry style.

It became apparent that the FP$_{122}$ cavity was unstable. A photograph of a bond interface for one mirror is shown in Fig. S2(a), where poor coverage is evident. The instability of FP$_{122}$ manifested as a high drift rate plus some hysteresis (in compressibility and expansivity). The general flavor of this instability is shown in Fig. S2(b), which shows the vacuum zero for the two cavities during separate argon isotherms. Compared to the FP$_{150}$ cavity of the main text, the FP$_{122}$ is about 8 times less stable.

Procedures outlined in the main text were attempted on the unstable FP$_{122}$, albeit with an unrefined procedure and only partial coverage of the isotherm. The helium results are shown in Fig. S2(c), and the argon results are shown in Fig. S2(d). Clearly, the initial demonstration of dispersion gas barometry was a failure: κ has a range of almost 1 % and ϵ_p suggests a $1 \times 10^{-4} \cdot p$ difference between the optical and mechanical pressure scales! Most problematic was the fact that regression of the helium data to a diffusion model yielded different (~ 0.5 %) permeation characteristics at the two frequencies. (Helium diffusion is discussed in Sect. IV below. Diffusion characteristics should be almost identical at two resonance frequencies.) The
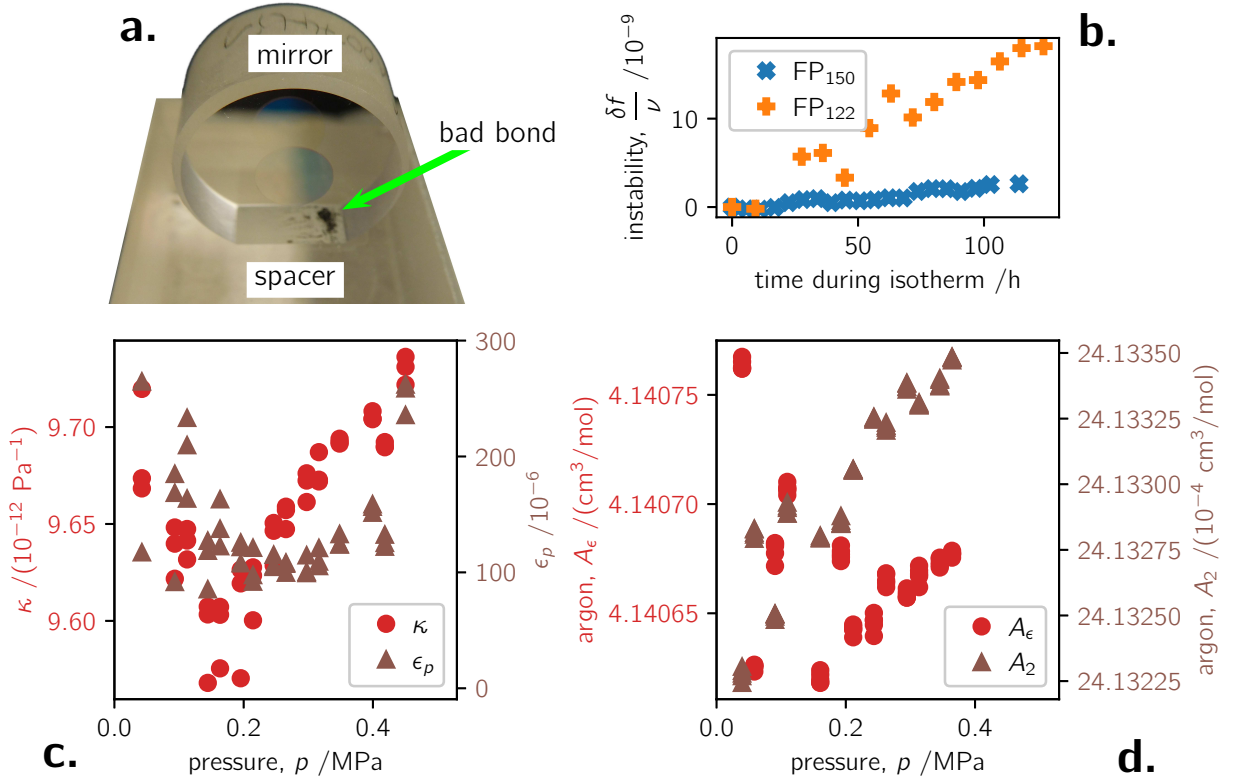

FIG. S2. Performance with an unstable cavity. (a.) A poor quality silicate bond on the FP$_{122}$ cavity. (b.) Temporal stability of the two cavities. (c.) Deduced parameters from the helium characterization. (d.) Deduced properties of argon.

origin of the helium problems was not clear, but it could be the combined effects of instability plus hysteresis together with a delay of almost 500 s between the vacuum zero resonance frequency and the first sample of the resonance frequency in helium. The inability to correctly account for diffusion at each resonance frequency partly explains the anomalously large ϵ_p. However, impurity of the helium used was later believed to cause at least half the ϵ_p value. [The Sect. V below discusses helium purity in more detail. It is also pointed out that the bad bond (void) area annotated in Fig. S2(a) might function as a trapped volume, and contribute additional impurity problems.]

The counterargument to declared failure is that the argon result is not too bad, and surprisingly close to the main text. The $3 \times 10^{-5} \cdot A_\epsilon$ range is nominally consistent with the ± 0.5 % variability on κ. The dispersion term differs from the main text by only $5 \times 10^{-5} \cdot A_2$, which is within the estimated uncertainty of the stable FP_{150} cavity performance. A final counterpoint is that the initial tests with FP_{122} were performed with an unrefined procedure, which allowed Δf for the 194 THz laser to vary as much as ± 1.4 GHz. With this unrefined procedure, the $\Delta f / \Delta \nu_{\mathrm{fsr}}$ of (S9) is problematic, and the deduced A_2 will fluctuate.

Hysteresis in compressibility is highly undesirable in a refractometer, as are long wait times between the initial vacuum state and the generated pressure state. And impurities in helium are about 20 times more problematic for dispersion gas barometry compared to single frequency refractometry. Nevertheless, in hindsight, the initial tests with the FP_{122} cavity were a stimulant to refine procedure rather than a failure.

IV. HELIUM DIFFUSION

From Crank [S4], it may be shown that permeation of helium into a rectangular block causes its fractional length to increase

$$\frac{\Delta L}{L} = \frac{HC}{3} \left[4 \left(\frac{D}{\pi} \right)^{\frac{1}{2}} \left(\frac{1}{l_x} + \frac{1}{l_y} + \frac{1}{l_z} \right) t^{\frac{1}{2}} - 16 \left(\frac{D}{\pi} \right) \left(\frac{l_x + l_y + l_z}{l_x l_y l_z} \right) t + 64 \left(\frac{D}{\pi} \right)^{\frac{3}{2}} \left(\frac{1}{l_x l_y l_z} \right) t^{\frac{3}{2}} \right] \quad \text{(S13)}$$

as a function of time t. The H is a conversion factor relating the amount of substance absorbed to the resultant fractional change in volume. The concentration $C = pS$ is given by solubility S and the gas pressure p, and D is the diffusion constant. The $l_{x,y,z}$ are the dimensions of the block, with $l_{x,y} = 28.6$ mm and $l_z = 180.3$ mm. The equation above is valid for short times; with $D = 1.52 \times 10^{-8}$ m^2/h at 23 °C [S5], the diffusion time-constants $l_{x,y,z}^2 / (\pi^2 D)$ exceed the $t < 0.5$ h analysis intervals of this work by four orders of magnitude. Although S and D are nominally known [S5] for the temperature of the present apparatus, H is unknown. Therefore, since $\Delta L / L \equiv -\Delta f / \nu$, the fractional change in resonance frequency

$$-\left(\frac{\Delta f}{\nu} \right)_\rho = \beta p \left(\sqrt{t} - 0.2827 \mathcal{D} t + 0.0158 \mathcal{D}^2 t^{3/2} \right), \quad \text{(S14)}$$

is described by a fit parameter $\beta = HS\mathcal{D}/3$ with a characteristic diffusion rate $\mathcal{D} = 4\sqrt{\frac{D}{\pi}} \left(\frac{1}{l_x} + \frac{1}{l_y} + \frac{1}{l_z} \right) = 0.021$ h$^{-\frac{1}{2}}$. The $(\Delta f / \nu)_\rho$ denotes the fractional change in resonance frequency adjusted to constant density ρ. In the framework $\Delta L = L_{\mathrm{gas}} - L_{\mathrm{vac}}$, β is signed positive.

An example of the helium diffusion transient is shown in Fig. S3 for a 0.28 MPa fill at the 474 THz resonance. In Fig. S3(a), the adjustment $(\Delta f / \nu)_\rho$ to constant density is predominantly for temperature, since the generated pressure is constant within $2 \times 10^{-7} \cdot p$. The gas temperature plotted has had a correction applied for the gradient between the resistance thermometer and cavity mode, based on the finite-element model of Fig. S1. Corrections greater than 30 μK only apply for $t < 0.11$ h. The (S14) fit to the data is shown in Fig. S3(a), and the residuals from the fit are in Fig. S3(b). Both the temperature and frequency data of Fig. S3(a) and (b) are relatively noisy because the averaging time is only 1 s. In this work, $\beta \approx 3 \times 10^{-14}$ Pa^{-1}h$^{-\frac{1}{2}}$, so an hour of exposure to helium causes a $10^{-4} \cdot (n - 1)$ error from the change in cavity length.

The parameter ϵ_p of the main text is immune to helium diffusion insofar as the change in (fractional) cavity length at both frequencies is identical. This work observed almost identical values for β at the two frequencies, and the differences are shown in Fig. S3(c). The labels "B," "C," "D," and "E" denote four separate helium isotherms with different purification treatments, detailed in the next section. Based on these data, the influence of diffusion on the determination of ϵ_p cancels to the level of $10^{-4} \cdot \beta$.
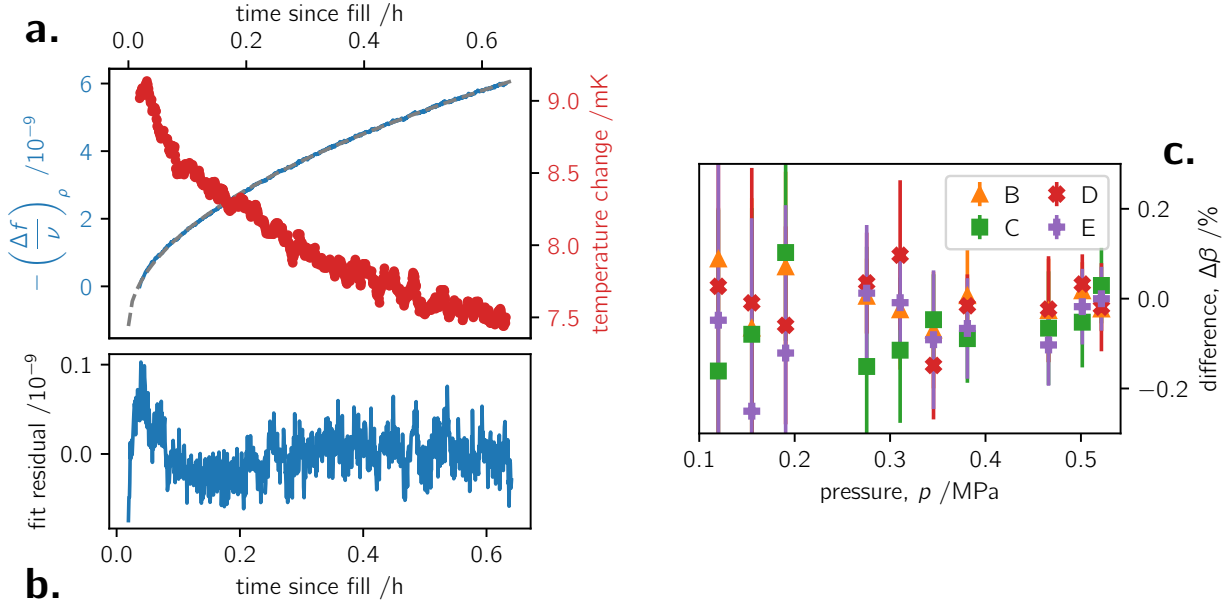
FIG. S3. Details about helium diffusion. (a.) Changes in fractional resonance frequency and temperature after a fill to 0.28 MPa. (b.) Residuals from a fit to (S14). (c.) Differences between the identified β at the two frequencies on separate isotherms. Errorbars span standard deviation on ten repeat measurements.

Effectively, dispersion gas barometry is about 50 times less sensitive to helium diffusion than single frequency refractometry. It is emphasized that this metric is only for identification of ϵ_p in helium. In the main text, the work with other gases relies on knowledge of κ to deduce A_ϵ. Identification of κ is prone to error in the application of (S14), and the extrapolation to time-zero after a fill, evident in Fig. S3(a).

V. HELIUM PURITY

Purity of helium is more problematic for dispersion gas barometry compared to single wavelength refractometry. At optical frequency, a contaminant like water [S6] has molar refractivity about 7.4 times larger than helium; however, the A_2 term of water is about 25 times larger than helium. Likewise, the more common contaminant hydrogen [S7] has A_ϵ only 4 times larger than helium; however, the A_2 term of hydrogen is about 14 times larger than helium. Impurity of the helium caused initial problems for this work, and the story toward a final result is told through Fig. S4. The plot shows gradual convergence to a final ϵ_p result for multiple helium isotherms featuring different purification treatments, labeled alphabetically. Details behind the helium purity trials are described in the next paragraph.

Two helium cylinders were purchased in 2020, and were specified as 99.9999 % purity. Gas chromatography in 2020 revealed the largest impurity to be hydrogen, which was present at the level of 0.18(10) µmol/mol. During 2022 and early 2023 one of the helium cylinders was depleted by 90 %, and remained so until the present work. The first helium measurements were undertaken on the unstable cavity of Sect. III in October 2024 using the 90 % depleted cylinder of helium without further purification. The result is plotted as "A" in Fig. S4. Although data with the unstable cavity might be viewed skeptically, it is believed that most of the $1.2 \times 10^{-4} \cdot \epsilon_p$ was caused by impurity. The conjecture is that over three years in a mostly depleted cylinder, hydrogen outgassing from the steel walls contaminated the helium at the level of 7 µmol/mol. After the result "A" with the unstable cavity, a helium isotherm was acquired with the FP_{150} cavity and the unused cylinder (till now), again without further purification. This result is plotted as "B" in Fig. S4. Again, the $6 \times 10^{-5} \cdot \epsilon_p$ suggests hydrogen outgassing over four years contaminated the helium over what was originally analyzed by gas chromatography. Next, an active getter was added to the manifold, still being supplied with the unused (till now) helium cylinder. The getter was specified to remove contaminants H_2O, O_2, H_2, CO, CO_2, CH_4 and N_2 to 10 nmol/mol. The getter-purified helium result is plotted as "C"
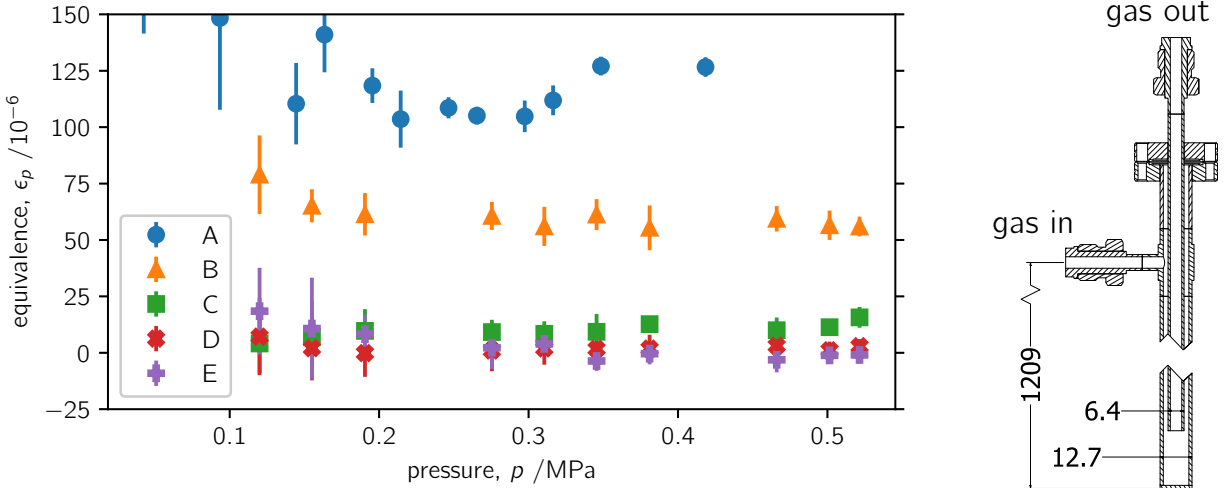
FIG. S4. Five helium isotherms with different purification treatments. (A) Unstable cavity result with unpurified helium from the old depleted cylinder. (B) Stable cavity result with unpurified helium from the old full cylinder. (C) Stable cavity result with getter-purified helium from an old full cylinder. (D) Stable cavity result with helium from an old full cylinder purified by a getter and liquid-helium coldtrap. (E) Stable cavity result using a new full cylinder purified by a getter and liquid-helium coldtrap. On right is a sketch of the coldtrap which was inserted into the liquid helium dewar.

in Fig. S4. Clearly, the getter improved the purity of helium supplied to the refractometer. However, a further step toward purity was taken by adding a liquid-helium coldtrap to the manifold, at the output of the getter. The coldtrap consisted of a tube within a tube, as sketched to the right of Fig. S4. The coldtrap was directly inserted into a 100 L dewar of liquid helium: the flow path was helium gas entered at the top of the 12.7 mm diameter assembly, flowed to the bottom, entered the 6.4 mm diameter assembly, flowed to the top, and exited to the refractometer apparatus. The getter- plus coldtrap-purified helium result is plotted as "D" in Fig. S4. There is a $6 \times 10^{-6} \cdot \epsilon_p$ offset between trends "C" and "D." The offset is a factor two larger than the precision deducing ϵ_p. Finally, a new cylinder of helium was purchased which was specified as 99.9999 % pure and featured a built-in purifier. The details behind the purifier are not fully known, but the claim is that it maintains H_2O below 20 nmol/mol, O_2 below 10 nmol/mol, and total hydrocarbons below 0.1 µmol/mol. The manufacturer provided a certificate of analysis showing the largest contaminant to be nitrogen at 0.2 µmol/mol, but no internal gas chromatography was carried out on this cylinder. This new cylinder fed the apparatus through the active getter plus coldtrap, and the result is plotted as "E" in Fig. S4. The results between trends "D" and "E" are consistent, which gives confidence that helium from different sources has been consistently purified. The offset between "C" compared to "D" and "E" suggests an active getter alone does not purify helium to the requisite levels.

The previous paragraph described the steps taken to ensure helium entering the refractometer was pure. The next concern would be impurities inside the refractometer apparatus, which might be released during a measurement. Apparatus impurity and acquisition time did not appear to influence the results. Recall first, all chamber fittings were sealed with differential pumped o-rings; gas and vacuum lines from the manifold were sealed with metal gaskets. Therefore, contamination entering the apparatus through seals was minimal. Also recall, the thermal response was rapid with helium data stable to within $3 \times 10^{-6} \cdot (n-1)$ after only 12 s. Data acquisition was fast—a single helium sample was acquired within 0.5 h, and each sample had a fresh fill of helium, which had been preceded by a pumpdown of the entire apparatus and manifold to high vacuum. Finally, any residual hydrogen or water outgassing into the pure helium volume would have manifested as discrepancies in the diffusion fit parameter β at the two resonance frequencies. There was no significant difference in β.

In summary, impurity of helium is probably the main systematic challenge for dispersion gas barometry. It took point of use purification plus a rapid thermal equilibration to achieve the present results.

VI.   UNCERTAINTY ANALYSIS

The uncertainty analysis follows the outline of the main text. First, the helium measurement will be treated. Technically, the helium measurement deduces two parameters ϵ_p and ΔL; however, it makes most sense to discuss helium uncertainty in terms of $p_{\mathrm{ops}} = (1 + \epsilon_p)p$ and $\kappa = (-\Delta L + \Delta L_\beta)/(p_{\mathrm{ops}}L)$. The main result of the helium measurement is realization of the optical pressure scale, and so $u(p_{\mathrm{ops}})$ is one interest. Subsequent measurements with other gases do not suffer diffusion, and so uncertainty in compressibility distortion $u(\kappa)$ is of main importance, rather than $u(\Delta L)$ which has the combined effects of distortion and diffusion.

After uncertainty in the helium result has been presented, the uncertainty deducing the polarizability parameters A_ϵ and A_2 for the other gases will be discussed. Throughout this supplement, the notation $u(x)$ is used to denote the standard uncertainty of the quantity x. Unless otherwise stated, all uncertainties in this work are one standard uncertainty, corresponding to approximately a 68 % confidence level.

A.   Helium: $p_{\mathbf{ops}}$ and κ

Most relevant optical and thermophysical properties for helium have been calculated by *ab initio* theory. (One minor exception is the frequency dependence of the third dielectric virial coefficient, which has negligible influence on this work.) The thermophysical properties B_ρ and C_ρ of helium [S8, S9] are known well enough to not significantly influence p_{ops} at these low pressures. The two-color approach is much more sensitive to the optical properties A_{R} [S10–S12], B_{R} [S13], and C_{R} [S14]. The Cauchy expansion for A_{R} [S11] had uncertainty estimates which suggested $u(p_{\mathrm{ops}})$ would be $3.8 \times 10^{-6} \cdot p$. However, the theory was later revised [S15] to include a so-called retardation correction factor. For the frequency separation of the present work, the retardation correction is a $4 \times 10^{-5} \cdot p$ increase in p_{ops}. The estimated relative uncertainty on the retardation correction is 0.025 % [S16]. The entry "He theory" in Table S-I reflects the combined contributions of the original estimate [S11] of A_2, plus its later retardation correction [S15].

Gas temperature was measured with a capsule-type standard platinum resistance thermometer (cSPRT), which carried ITS-90 calibration coefficients. A lengthy description of how well a calibrated cSPRT might infer gas temperature along a laser beam is given in Ref. [S2], and the estimated uncertainty is 0.3 mK. Converting a temperature measured on ITS-90 to thermodynamic temperature [S17] incurs a further 0.7 mK uncertainty. These two components are added in quadrature to produce the entry in Table S-I.

As mentioned in the main text, the two-color method requires the pressure input to Eq. (8) known within ± 3.2 kPa to identify Δm, which corresponds to 1 % at 0.5 MPa. So long as this modest requirement is satisfied, $p_{\mathrm{ops}} \equiv (1 + \epsilon_p)p$ is independent of the initial estimate of p, with ϵ_p being the optimized calibration factor. Consequently, realizing p_{ops} is largely independent of the mechanical pressure scale, and the entry for pressure in Table S-I is blank. Likewise, for a single quadruplet, the ΔL solved in Eq. (6) is independent of pressure. However, use of a (practical) distortion coefficient in other gases must use the optical pressure $\kappa = (-\Delta L + \Delta L_\beta)/(p_{\mathrm{ops}}L)$. Therefore, uncertainty using κ in other gases inherits $u(p_{\mathrm{ops}})$, which explains the pressure entry in Table S-I.

TABLE S-I. Relative standard uncertainty for parameters deduced by the helium measurement.

component	$u_{\mathrm{r}}(p_{\mathrm{ops}})$ /10^{-6}	$u_{\mathrm{r}}(\kappa)$ /10^{-4}
He theory $A_{\mathrm{R}}(\nu), B_\rho, \ldots$	4.0	< 0.1
temperature T	2.5	< 0.1
pressure p	—	1.0
frequency $\Delta f/\Delta \nu_{\mathrm{fsr}}$	0.2	< 0.1
diffusion β	0.6	0.2
impurity	0.7	0.2
statistical	3.0	1.7
combined $k = 1$	5.7	2.0

The comb-based clockwork described in the main text allows $(\Delta f_{\text{red}} - \Delta f_{\text{blue}})$ to be measured within about 50 mHz. Problems in frequency metrology caused by using a finesse 2000 cavity are many orders of magnitude larger than the precision of the comb-based clockwork. As stated around Eq. (6) of the main text, the method strategically selected pressures that minimized Δf for both frequencies. The reason behind this strategy is that the quotient of the measured frequencies $\Delta f / \Delta\nu_{\text{fsr}}$ in Eq. (6) has statistical error in Δf and systematic error in $\Delta\nu_{\text{fsr}}$. The statistical contribution to the measured changes in resonance frequencies $u(\Delta f)$ is absorbed into the "statistical" uncertainty entry described below. This paragraph is concerned with the systematic uncertainty in the free spectral range $\Delta\nu_{\text{fsr}}$, a measured characteristic of the cavity. The $\Delta\nu_{\text{fsr}}$ was measured by locking two lasers to adjacent modes of the cavity. The 474 THz lasers had tuning of less than 1.2 GHz, so locking was possibly to only two adjacent modes. Switching the lasers between the two accessible modes showed offsets of almost 1 kHz in $\Delta\nu_{\text{fsr}}$. A better estimate was provided by the 194 THz lasers, because their 8 GHz tuning range allowed evaluations of $\Delta\nu_{\text{fsr}}$ separated by up to eight modes. Consequently, the influence of offsets were reduced by eight. The differences between the $\Delta\nu_{\text{fsr}}$ measured at the two frequencies was within 10 % of what was expected from knowledge of the mirror reflection phase-shift. The overall estimate $u(\Delta\nu_{\text{fsr}})$ was 200 Hz, or 2×10^{-7} in fractional terms. Since the procedure kept $|\Delta f / \Delta\nu_{\text{fsr}}| < 0.05$ at both frequencies, the frequency quotient may contribute systematic errors of $10^{-8} \cdot (n-1)$ to the numerator of Eq. (6). For helium pressures around 0.3 MPa, the other term in the numerator is $\Delta m > 15$. So, at a single frequency, systematic error in the frequency quotient represents a 7×10^{-10} uncertainty. The entry in Table S-I for $u(p_{\text{ops}})$ reflects the fact that an uncertainty contributor to single frequency refractivity is amplified by $A_{\text{R}}/\Delta A_{\text{R}} = 206$ in the present demonstration.

One attraction of the two-color determination of p_{ops} is that changes in cavity length common at both frequencies largely cancel. The cancellation affords immunity to compressibility, helium diffusion, thermal expansion, and dimensional drift. Of main concern is helium diffusion, which was detailed in Section IV above. For $u(p_{\text{ops}})$, the question is to what level does diffusion cancel at both frequencies. An answer to this question was provided by studying the similarity of β at the two cavity resonance frequencies. The Fig. S3(c) placed a firm bound on $\Delta\beta$: the difference in the diffusion trend is less than 10^{-4}. The contribution of diffusion to $u(p_{\text{ops}})$ is determined by this estimate of similarity in β. (Diffusion changes cavity length by about 10^{-10} /s. The objective to measure relative changes in optical length to the level of 10^{-13} means that the counters measuring each resonance frequency must be synchronized within 1 ms.)

The second concern with diffusion is that subsequent measurements with other gases require $\kappa = (-\Delta L + \Delta L_\beta)/(p_{\text{ops}}L)$. The ΔL is the actual parameter deduced from the helium measurement. Solving for κ depends on how well $\Delta L_\beta = \beta p \sqrt{t} L$ may be extrapolated to the time immediately after a fill. An example of this extrapolation is shown in Fig. S3(a). Systematic errors affecting β are mostly related to timing. Though all data acquisition is timed to 1 s, it is possible that the time axis of Fig. S3(a) could be offset by 10 s. A timing offset causes $2.7 \times 10^{-5} \cdot \kappa$ error. A second error relating to timing is the omission of some initial data when regressing to (S14). Finite-element based corrections are applied for the initial temperature disturbance from the gas fill. Nevertheless, the first few datapoints after a fill appear as outliers from (S14). In this work, datapoints within 45 s of the fill are omitted from the regression to (S14). Omitting data within 15 s of the fill causes $2.0 \times 10^{-6} \cdot \kappa$ error. (The rapid thermal response highlighted in Sect. II is reemphasized. In helium, finite-element analysis predicts that gradients between the thermometer and cavity mode have dropped below 1 mK after 12 s for a 0.1 MPa. A rapid thermal response allows reliable extrapolation of the diffusion trend, witnessed via the constant density change in resonance frequency.) A final systematic contributor to $u(\kappa)$ is error in the diffusion model. The (S14) is the explicit solution for a block of specified dimensions. However, the FP cavity differs from a block because the two D-shaped mirrors are stood up on the block [see Fig. S1 and Fig. S2(a)]. It would be difficult to derive an explicit solution for diffusion in the FP cavity geometry. As a worst case, it is assumed that diffusion in the FP cavity follows something between the block model of (S14) and the rod model $-(\Delta f/\nu)_\rho = \beta\left(\sqrt{t} - \mathcal{D}\frac{\pi}{16}t\right)$ [S4]. Error in the diffusion model is an influence below $2 \times 10^{-6} \cdot \kappa$. Last and least significant, higher order terms in (S14) are influenced by the characteristic diffusion rate $\mathcal{D}$ which is subject to error in the block dimensions and the reference value used for the diffusion constant [S5]. A 10 % uncertainty on $\mathcal{D}$ is conservative, and it influences the extrapolation below $10^{-6} \cdot \kappa$. The entry for β in Table S-I covers systematic uncertainty. In practice, diffusion contributes larger statistical effects, but these are covered by the statistical entry.

The efforts taken to ensure helium impurity are described in Sect. V. The increased sensitivity of dispersion gas barometry to impurity (compared to single wavelength refractometry) is arguably its one disadvantage. Achieving the sub-$10^{-6} \cdot p$ uncertainty of this work required point of use purification and rapid cycle times. The uncertainty assigned in Table S-I to impurity is based on half the range of the average difference in

the ϵ_p deduced in the helium isotherms "D" and "E," which employed cylinders from different suppliers, but which underwent the same point of use purification. This evaluation is imperfect because (i) between isotherms ϵ_p is only as reproducible as the refractometer and piston gage, and (ii) the actual purity level of helium is not tested inside the apparatus. Nevertheless, the evaluation is reasonable. Arguably, the active getter plus a helium coldtrap ought to deliver the highest possible purity. And confidence is added by the fact that consistent results for ϵ_p are obtained from different cylinders feeding the same purification system.

The statistical entries for p_{ops} and κ were estimated as the standard deviation of the mean across all set pressures. For κ, this evaluation is fairly reasonable. The compressibility of fused quartz glass is expected [S18] to fractionally increase by 1.6×10^{-4} MPa^{-1}, which is within the precision of the κ determination at pressures below 0.5 MPa. For p_{ops}, in principle ϵ_p needs to follow a function that corrects the initial p estimate to the optical pressure scale. In the present demonstration, the estimated p is from a highly accurate piston gage [S19]. The expected mean value of ϵ_p is about $2 \times 10^{-6} \cdot p$, chiefly because of uncertainty on the diameter of the piston gage. The ϵ_p might also take a linear trend as a function of pressure because of uncertainty in the distortion coefficient of the piston gage, but this trend is not expected to exceed $0.4 \times 10^{-6} \cdot p$ up to 0.5 MPa. These expected values of ϵ_p are below the resolution of the present demonstration; consequently, standard deviation of the mean is also a reasonable evaluation of statistical uncertainty in p_{ops}. It is pointed out that the errorbars on the ϵ_p data of Fig. 2 in the main text correspond to standard deviation of 10 repeats at each set pressure. The average span of the errorbars is $8.2 \times 10^{-6} \cdot p$. The errorbars in Fig. 2 increase as pressure decreases. The most likely cause of increased deviation at low pressure is frequency instability.

B.   Other gases: A_ϵ and A_2

In Table S-II, the entries for $u(T)$, $u(\Delta f/\Delta \nu_{\text{fsr}})$, and $u(\kappa)$ were treated in the previous subsection. Only two things need be added. First, for a given pressure change, gases with higher polarizability produce a larger change in cavity mode number Δm in (S9). Consequently, the influence of $u(\Delta f)$ and $u(\kappa)$ is smaller for gases other than helium. Second, and likewise, other gases do not suffer diffusion, and perturbations to cavity length during the measurement have a smaller overall effect.

Determination of A_ϵ is completely dominated by the first entry in Table S-II. The p_{ops} is based on the helium measurements of this work, and its uncertainty was described in the previous subsection. The $u(p_{\text{ops}})$ is state-of-the-art. The present work features a mechanical pressure generator with $u(p) \approx 2 \times 10^{-6} \cdot p$, which would afford a more accurate determination of A_ϵ. However, there is an important metrological concept behind reporting the properties of neon, argon, and nitrogen on p_{ops}. The metrological concept concerns "quantity of like kind". If the properties of neon, argon, and nitrogen are referenced to the mechanical pressure generator, subsequent use of these properties merely establishes an optical pressure scale traceable to the diameter of a piston gage. The point might seem moot, but the large uncertainty on A_ϵ accurately reflects the uncertainty in an optical pressure scale that is independent of either the diameter of a piston gage or the density of mercury.

TABLE S-II. Relative standard uncertainty for parameters deduced in the measurement of neon, argon, and nitrogen.

component	neon $u_{\text{r}}(A_\epsilon)$ /10^{-6}	neon $u_{\text{r}}(A_2)$ /10^{-5}	argon $u_{\text{r}}(A_\epsilon)$ /10^{-6}	argon $u_{\text{r}}(A_2)$ /10^{-5}	nitrogen $u_{\text{r}}(A_\epsilon)$ /10^{-6}	nitrogen $u_{\text{r}}(A_2)$ /10^{-5}
pressure p_{ops}	5.7	—	5.7	—	5.7	—
temperature T	2.5	—	2.5	—	2.5	—
Cauchy coefficients $A_{4,6}$	< 0.1	2.9	< 0.1	2.5	0.4	19.8
magnetic susceptibility A_μ	< 0.1	—	< 0.1	—	< 0.1	—
virial coefficient B_{R}, B_ρ	< 0.1	< 0.1	< 0.1	< 0.1	< 0.1	< 0.1
frequency $\Delta f/\Delta \nu_{\text{fsr}}$	< 0.1	2.0	< 0.1	0.5	< 0.1	0.5
cavity distortion κ	3.3	—	0.8	—	0.7	—
impurity	4.0	0.1	0.1	0.1	0.1	0.1
statistical	0.6	0.9	1.0	2.2	0.8	2.6
combined $k = 1$	8.3	3.6	6.4	3.4	6.3	20.0

The influence of the Cauchy coefficients was numerically evaluated by performing the root-finding analysis with standard error added to $A_{4,6}$. The estimated standard errors in A_4 were 0.28 % for neon [S20] and 0.12 % for argon [S21]. These estimates are based on detailed uncertainty budgets from *ab initio* calculation. For nitrogen, the A_4 from the dipole oscillator strength sums [S22] has a minimal statement of < 1 % uncertainty. Using argon as a guideline, the A_4 from the dipole oscillator strength sums of argon differed from *ab initio* calculation by 0.6 % [S21]. Therefore, $u(A_4) = 1$ % for nitrogen seems reasonable to assume.

Uncertainty in magnetic susceptibility is a vexing question. At present, *ab initio* calculation of helium [S12], neon [S23], and argon [S23] all have stated uncertainties that would allow optical refractivity measurements to infer static polarizability well below $10^{-7} \cdot A_\epsilon$. However, these *ab initio* calculations all exhibit deviations of 6 % to 9 % from the measurement of A_μ due to Barter et al. [S24] in 1960. A 10 % error in A_μ would cause optical refractivity measurements to misidentify static polarizability by about $2 \times 10^{-6} \cdot A_\epsilon$. For nitrogen, the recent *ab initio* calculation [S25] is 50 % larger than experimental work [S26] from almost 100 years ago. This work assumes A_μ from *ab initio* calculation is more reliable than experiment for all gases. This assumption leads to the uncertainties of Table S-II, which might not be on solid ground. The importance of a precision measurement of A_μ can not be understated.

The second density B_ρ and refractivity B_R virial coefficients have weak influence on the results, so long as $A_\epsilon(p)$ and $A_2(p)$ are extrapolated to zero pressure. Knowledge of B_ρ is as good as 0.021 cm^3/mol for neon from *ab initio* calculation [S27], and has an accurate experimental validation by dielectric constant gas thermometry. For argon and nitrogen, knowledge of B_ρ is at the level of 0.027 cm^3/mol and 0.046 cm^3/mol, respectively, by the measurement technique of refractive index gas thermometry [S2]. The second refractivity virial coefficient B_R has been calculated [S13] for neon and argon. For neon, the pair polarizability underlying B_R has no estimate of uncertainty. Consequently, B_R has no estimate of uncertainty, but it is consistent with measurements within 0.05 cm^6/mol^2.

Argon and nitrogen have similar polarizability (and dispersion) to typical contaminants. They are also readily available in 99.9999 % purity. These two facts mean that impurity in argon and nitrogen has small influence on the overall uncertainty. Neon is different—it has lower polarizability dispersion than typical contaminants, and it is not commercially available at better than 99.9995 % purity. (For this work, 99.9995 % purity was difficult to procure.) An ambient temperature purifier was used when neon was fed to the manifold. The purifier was specified to remove H_2O, O_2, CO, CO_2, H_2, and $C_{>5}$-hydrocarbons. The purifier did not remove nitrogen, nor helium and argon. The neon was supplied with an analysis certificate which showed the largest contaminant to be H_2O at 0.8 µmol/mol; N_2 was specified at 13 nmol/mol. However, both argon and helium were specified by limits not to exceed 1.0 µmol/mol and 3.0 µmol/mol, respectively. Since the purifier removed H_2O, impurity in the neon was dominated by the limit-specified amounts of argon and helium. For both A_ϵ and A_2, the combined effects of argon and helium on neon at the limit-specified levels would largely cancel. However, these are bias effects without exact specification. Consequently, the entries in the table assume neon could be contaminated by up to 1.0 µmol/mol of argon.

For statistical entries $u(A_2)$ in Table S-II, a linear fit was applied to the data of Fig. 3 of the main text to extrapolate $A_2(p)$ to zero density. The uncertainty in the fit was estimated as the square root of the covariance matrix.

[S1] J. R. Lawall, High resolution determination of radii of curvature using Fabry–Perot interferometry, Measurement Science and Technology **20**, 045302 (2009).

[S2] P. F. Egan and Y. Yang, Optical $n(p, T_{90})$ measurement suite 1: He, Ar, and N_2, International Journal of Thermophysics **44**, 181 (2023).

[S3] I. Silander, J. Zakrisson, V. S. de Oliveira, C. Forssén, A. Foltynowicz, T. Rubin, M. Zelan, and O. Axner, *In situ* determination of the penetration depth of mirrors in Fabry-Perot refractometers and its influence on assessment of refractivity and pressure, Optics Express **30**, 25891 (2022).

[S4] J. Crank, The mathematics of diffusion (Clarendon Press, Oxford, 1975) Chap. 5, 2nd ed.

[S5] S. Avdiaj, Y. Yang, K. Jousten, and T. Rubin, Note: Diffusion constant and solubility of helium in ULE glass at 23 °C, The Journal of Chemical Physics **148**, 116101 (2018).

[S6] P. F. Egan and Y. Yang, Optical $n(p, T_{90})$ measurement suite 2: H_2O and D_2O, International Journal of Thermophysics **45**, 89 (2024).

[S7] J. Rychlewski, Frequency dependent polarizabilities for the ground state of H_2, HD, and D_2, The Journal of Chemical Physics **78**, 7252 (1983).

[S8] P. Czachorowski, M. Przybytek, M. Lesiuk, M. Puchalski, and B. Jeziorski, Second virial coefficients for ^{4}He and ^{3}He from an accurate relativistic interaction potential, Physical Review A **102**, 042810 (2020).

[S9] D. Binosi, G. Garberoglio, and A. H. Harvey, Third density and acoustic virial coefficients of helium isotopologues from *ab initio* calculations, The Journal of Chemical Physics **160**, 244305 (2024).

[S10] M. Puchalski, K. Szalewicz, M. Lesiuk, and B. Jeziorski, QED calculation of the dipole polarizability of helium atom, Physical Review A **101**, 022505 (2020).

[S11] M. Puchalski, K. Piszczatowski, J. Komasa, B. Jeziorski, and K. Szalewicz, Theoretical determination of the polarizability dispersion and the refractive index of helium, Physical Review A **93**, 032515 (2016).

[S12] M. Puchalski, M. Lesiuk, and B. Jeziorski, Relativistic treatment of the diamagnetic susceptibility of helium, Physical Review A **108**, 042812 (2023).

[S13] G. Garberoglio and A. H. Harvey, Path-integral calculation of the second dielectric and refractivity virial coefficients of helium, neon, and argon, Journal of Research of National Institute of Standards and Technology **125**, 125022 (2020).

[S14] G. Garberoglio, A. H. Harvey, J. Lang, M. Przybytek, M. Lesiuk, and B. Jeziorski, Path-integral calculation of the third dielectric virial coefficient of helium based on *ab initio* three-body polarizability and dipole surfaces, The Journal of Chemical Physics **161**, 144111 (2024).

[S15] K. Pachucki and M. Puchalski, Refractive index and generalized polarizability, Physical Review A **99**, 041803 (2019).

[S16] Personal correspondance with Mariusz Puchalski, February 2025.

[S17] C. Gaiser, B. Fellmuth, R. M. Gavioso, M. Kalemci, V. Kytin, T. Nakano, A. Pokhodun, P. M. C. Rourke, R. Rusby, F. Sparasci, P. P. M. Steur, W. L. Tew, R. Underwood, R. White, I. Yang, and J. Zhang, 2022 update for the differences between thermodynamic temperature and ITS-90 below 335 K, Journal of Physical and Chemical Reference Data **51**, 043105 (2022).

[S18] M. Vukcevich, A new interpretation of the anomalous properties of vitreous silica, Journal of Non-Crystalline Solids **11**, 25 (1972).

[S19] P. F. Egan, E. S. Stanfield, J. R. Stoup, and C. W. Meyer, Conversion of a piston–cylinder dimensional dataset to the effective area of a mechanical pressure generator, Metrologia **61**, 065004 (2024).

[S20] M. Lesiuk, M. Przybytek, and B. Jeziorski, Theoretical determination of polarizability and magnetic susceptibility of neon, Physical Review A **102**, 052816 (2020).

[S21] M. Lesiuk and B. Jeziorski, First-principles calculation of the frequency-dependent dipole polarizability of argon, Physical Review A **107**, 042805 (2023).

[S22] A. Kumar and W. J. Meath, Constrained anisotropic dipole oscillator strength distribution techniques, and reliable results for anisotropic and isotropic dipole molecular properties, with applications to H_2 and N_2, Theoretica Chimica Acta **82**, 131 (1992).

[S23] M. Lesiuk and B. Jeziorski, Diamagnetic susceptibility of neon and argon including leading relativistic effects, Physical Review A **109**, 012820 (2024).

[S24] C. Barter, R. G. Meisenheimer, and D. P. Stevenson, Diamagnetic susceptibilities of simple hydrocarbons and volatile hydrides, The Journal of Physical Chemistry **64**, 1312 (1960).

[S25] M. Lesiuk and J. Lang, Atomic Bethe logarithm in the mean-field approximation, Physical Review A **108**, 042817 (2023), calculated A_μ data for nitrogen at: `https://doi.org/10.5281/zenodo.10960043`.

[S26] G. G. Havens, The magnetic susceptibilities of some common gases, Physical Review **43**, 992 (1933).

[S27] R. Hellmann, C. Gaiser, B. Fellmuth, T. Vasyltsova, and E. Bich, Thermophysical properties of low-density neon gas from highly accurate first-principles calculations and dielectric-constant gas thermometry measurements, The Journal of Chemical Physics **154**, 164304 (2021).